Dalton Transactions

PAPER

View Article Online
View Journal | View Issue

Cite this: *Dalton Trans.*, 2017, **46**, 6912

Cu(III)triarylcorroles with asymmetric push–pull *meso*-substitutions: tunable molecular electrochemically catalyzed hydrogen evolution†

Xu Liang, *[a] Yingjie Niu,[a] Qianchong Zhang,[b] John Mack, *[c] Xiaoyi Yi,[d] Zweli Hlatshwayo,[c] Tebello Nyokong,[c] Minzhi Li[a] and Weihua Zhu*[a]

Received 27th February 2017,
Accepted 6th April 2017

DOI: 10.1039/c7dt00716g

rsc.li/dalton

The synthesis of four low symmetry A_2B type Cu(III)triarylcorroles with *meso*-aryl substituents that provide electron donating (push) and withdrawing (pull) properties is reported, along with their structural characterization by NMR spectroscopy and X-ray crystallography. An analysis of the structure–property relationships in the optical and redox properties has been carried out by comparing their optical spectroscopy, electrochemistry, and spectroelectrochemistry to trends predicted in DFT and TD-DFT calculations. The results demonstrate that A_2B type Cu(III)triarylcorroles are highly efficient catalysts for electrocatalyzed hydrogen evolution reactions (HERs) and that their reactivity can be modulated by changing the nature of the B-position *meso*-substituent.

Introduction

Rational control of the electronic structure of chromophores through the introduction of substituents or changes in molecular symmetry has been central to the design of functional molecular dyes.[1] The importance of this approach has increased significantly due to its importance in various fields such as molecular catalysis and photo-energy conversion, and this has led to significant interest in the further structural modification of organic dye chromophore molecules.[2] Push–pull strategies involve the introduction of both electron-donating (push) and withdrawing (pull) substituents. This has been shown to enable significant modifications to the electronic structures of porphyrins, phthalocyanines, and corroles.[3] Large shifts in the wavelengths of the main spectral bands and in the redox potentials are often observed that can be readily rationalized through a consideration of how the differing alignments of the angular nodal patterns of the frontier π-MOs of the porphyrinoid macrocycle modify the effect of introducing the substituents.[3a,d,e] The goal of this study is to investigate whether the introduction of a push–pull *meso*-aryl substitution pattern has a significant effect on the electrocatalytic properties of Cu(III)corroles.

The use of hydrogen for energy storage so that supply from renewable sources can be balanced with demand through the use of fuel cells has many advantages and is widely considered to be the energy source that is most likely to replace the use of fossil fuels in many contexts.[1,4] There has been increasing interest in hydrogen evolution reactions (HERs) that involve the electrochemical reduction of protons, due to the straightforward procedures that are involved and the availability of catalytic materials to convert electrical energy to chemical energy through the generation of H_2 gas.[5] Recent research has indicated that molecular electrochemical catalysis exhibits various advantages, including high efficiency or tunable catalytic efficiency and the stability of the molecular catalysts.[4b,6] In this kind of study, the modulation of HER reactions has recently been achieved through molecular electrochemical catalysis by singly or doubly electrochemically reduced metalloporphyrins and metallo-corroles, and the catalytic efficiency can be modulated by the symmetric and asymmetric introduction of various substituents.[7]

Although several molecular catalysts act as efficient electrocatalysts for HERs, the use of porphyrinoid chromophores with asymmetric push–pull *meso*-substituents has yet to be explored. A_2B type low symmetry corroles (Scheme 1) with push–pull substituents are obvious candidates to study in this context, since various push–pull systems can be readily

[a]*School of Chemistry and Chemical Engineering, Jiangsu University, Zhenjiang 212013, P. R. China. E-mail: liangxu@ujs.edu.cn, sayman@ujs.edu.cn*
[b]*State Key Laboratory of Physical Chemistry of Solid Surface and Department of Chemistry, College of Chemistry and Chemical Engineering, Xiamen University, Xiamen 361005, P. R. China*
[c]*Department of Chemistry, Rhodes University, Grahamstown 6140, South Africa. E-mail: j.mack@ru.ac.za*
[d]*School of Chemistry and Chemical Engineering, Central South University, Changsha 410083, P. R. China*

†Electronic supplementary information (ESI) available: Structural characterization and theoretical calculation data. CCDC 1534791. For ESI and crystallographic data in CIF or other electronic format see DOI: 10.1039/c7dt00716g

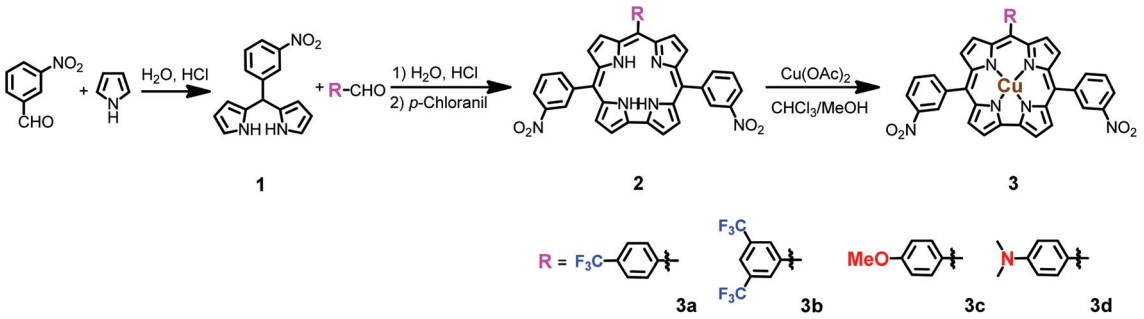

Scheme 1 Synthesis of Cu(III)-*meso*-triarylcorroles.

prepared through the use of different arylaldehyde precursors (Scheme 1). In this manuscript, the synthesis of a series of low symmetry A_2B type Cu(III)corroles is described, along with their structural characterization, and an analysis of their electronic structures and their suitability for use as molecular catalysts for HER reactions.

Experimental

General

^1H and ^{19}F NMR spectra were recorded on a Bruker AVANCE 400 spectrometer (400.03 MHz). Residual solvent peaks were used to provide internal references for the ^1H NMR spectra (δ = 7.26 ppm for $CDCl_3$, δ = 5.32 ppm for CD_2Cl_2). All reagents and solvents used were of reagent grade and were used as received unless noted otherwise. Cyclic voltammetry was carried out on a Chi-730D electrochemistry station with a three-electrode cell. A glassy carbon disk, a platinum wire and an Ag/AgCl electrode were used as the working, counter and reference electrodes, respectively. The UV and visible regions of the electronic absorption spectra were recorded with an HP 8453A diode array spectrophotometer, while a Shimadzu UV-3600 Plus instrument was used for measurements in the NIR region. An optically transparent thin-layer cell that was built in house was used to carry out spectroelectrochemistry. Measurements were performed by attaching the Pt mesh working electrode to a Chi-730D electrochemical working station. An inert nitrogen atmosphere was introduced during all of the electrochemical and spectroelectrochemical measurements, which were carried out at room temperature. A JASCO J-815 spectrodichrometer equipped with a JASCO permanent magnet (1.6 tesla) was used to record magnetic circular dichroism (MCD) spectra. Spectra were recorded using both parallel and antiparallel fields. The conventions recommended by Piepho and Schatz are used to describe the sign of the Faraday terms, so the sign of the $\mathbf{B_0}$ terms matches that of the MCD signal.[8]

X-ray crystal structure

A single crystal of X-ray diffraction quality of **3d** was grown in a $CHCl_3$ and MeOH solution. Data were collected with Mo-K_α radiation (λ = 0.71073 Å) by using a Saturn 724 instrument. The structure (Fig. 1) was solved by direct methods. Non-hydrogen atoms were refined anisotropically by least-squares on F^2 using the SHELXTL-97 program,[9] and hydrogen atoms of the molecule were generated geometrically (C–H, 0.96 Å). CCDC number: 1534791 contain the supplementary crystallographic data for **3d**.

Computational methods

The Gaussian 09 software package[10] was used to carry out DFT geometry optimizations for **3a–d** and model complexes with *meso*-phenyl rings at only the B-position (**1Ph**) and at the A_2- and B-positions (**3Ph**) by using the B3LYP functional with 6-31G(d) basis sets. Slightly saddled structures were predicted with N–M–N angles in the central cavity of below 10° for **3a** (3.4 and 3.7°). TD-DFT calculations were carried out by using CAM-B3LYP functional, which includes a long-range correction of the exchange potential, since this provides more accurate results for complexes that have excited states with a significant intramolecular charge transfer character.

Synthesis and characterization

Synthesis of Cu(III)-5,15-(*m*-nitrophenyl)-10-trifluoromethylphenylcorrole (3a). 5,15-(*m*-Nitrophenyl)-10-phenylcorrole (0.05 mmol, 0.0308 g)[11] and $CuAc_2$ (0.25 mmol, 0.0623 g) were

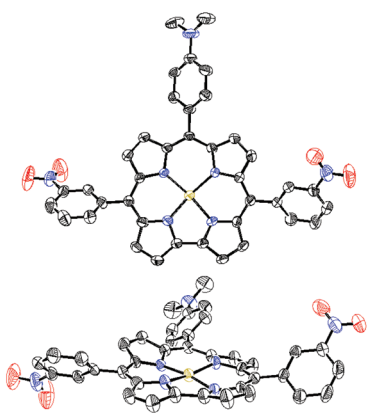

Fig. 1 Single crystal X-ray structure of **3d**, top (up) and side views (bottom) with thermal ellipsoids set at 50% probability and with protons and solvent molecules removed.

dissolved in a mixture of 5 mL $CHCl_3$ and 20 mL methanol, which was then stirred and heated at 75 °C under N_2 for 1 h. After removal of the solvent, the residue was further purified by Al_2O_3 gel chromatography (eluent: CH_2Cl_2/hexane = 1 : 1), and the target compound was obtained in 86.3% yield (0.0290 g). MALDI-TOF-MS: m/z = 745.52 (calcd $[M]^+$ = 745.14). ^{1}H NMR (CD_2Cl_2, 298 K): δ = 8.64 (2H, s), 8.46 (2H, d; J = 8.0 Hz), 8.10 (2H, d; J = 8.0 Hz), 7.88 (2H, d; J = 4.0 Hz), 7.70–7.59 (6H, m), 7.46 (2H, d; J = 4.4 Hz), 7.28 (2H, d; J = 4.4 Hz), 6.79 (2H, d; J = 4.4 Hz), 3.06 ppm (6H, s). ^{19}F NMR ($CDCl_3$, 298 K): δ = −62.57 (3F, s).

Cu(III)-5,15-(*m*-Nitrophenyl)-10-3,5-bistrifluoromethylphenylcorrole (3b). The synthetic procedure for **3b** was identical to that for **3a**, with H_3-5,15-(*m*-nitrophenyl)-10-(3,5-bistrifluoromethyl-phenyl)corrole **2b** used in place of **2a**. The target compound was obtained in 90.2% yield (0.0281 g). MALDI-TOF-MS: m/z = 813.35 (calcd $[M]^+$ = 813.14). ^{1}H NMR ($CDCl_3$, 298 K): δ = 8.61 (2H, s), 8.47 (2H, d; J = 8.0 Hz), 8.11 (3H, s), 8.07 (2H, d; J = 8.0 Hz), 7.98 (2H, d; J = 4.0 Hz), 7.71 (2H, t; J_1 = J_2 = 8.0 Hz), 7.60 (2H, d; J = 4.0 Hz), 7.29 (2H, d; J = 4.0 Hz), 7.16 (2H, d; J = 4.0 Hz). ^{19}F NMR ($CDCl_3$, 298 K): δ = −62.63 (3F, s).

Cu(III)-5,15-(*m*-Nitrophenyl)-10-*p*-methoxyphenylcorrole (3c). The synthetic procedure for **3c** was identical to that for **3a**, with H_3-5,15-(*m*-nitrophenyl)-10-(*p*-methoxyphenyl)corrole **2c** used in place of **2a**. The target compound was obtained in 90.2% yield (0.0281 g). MALDI-TOF-MS: m/z = 707.22 (calcd $[M]^+$ = 707.17). ^{1}H NMR ($CDCl_3$, 298 K): δ = 8.62 (2H, s), 8.45 (2H, d; J = 8.0 Hz), 8.08 (2H, d; J = 8.0 Hz), 7.90 (2H, d; J = 3.2 Hz), 7.71–7.57 (6H, m), 7.36 (2H, d; J = 4.0 Hz), 7.28 (2H, s), 7.00 (2H, d; J = 4.4 Hz), 3.99 ppm (3H, s).

Synthesis of Cu(III)-5,15-(*m*-nitrophenyl)-10-*p*-dimethylamino-phenylcorrole (3d). The synthetic procedure was identical to that for **3a**, with H_3-5,15-(*m*-nitrophenyl)-10-(*p*-dimethylamino-phenyl)corrole **2d** used in place of **2a**. The target compound was obtained in 63.2% yield (0.0281 g). MALDI-TOF-mass: m/z = 720.35 (calcd $[M]^+$ = 720.21). ^{1}H NMR ($CDCl_3$, 298 K): δ = 8.64 (2H, s), 8.46 (2H, d; J = 8.0 Hz), 8.10 (2H, d; J = 8.0 Hz), 7.88 (2H, d; J = 4.0 Hz), 7.71–7.59 (6H, m), 7.46 (2H, d; J = 8.0 Hz), 7.29 (2H, d; J = 4.0 Hz), 6.79 (2H, d; J = 8.0 Hz), 6.50 (2H, br s), 3.06 ppm (6H, s).

Results and discussion

Synthesis and characterization

The free base corrole compounds (**2a–d**) were synthesized from a reaction of dipyrromethane **1** and the appropriate aryl-aldehyde (Scheme 1) according to the literature procedures.[11] Cu(III)corroles (**3a–d**) were then synthesized by a metalation reaction of **2a–d**, and were purified by silica gel column chromatography and recrystallization. MALDI-TOF MS for **3a** revealed an intense parent peak at m/z = 745.52 (calcd $[M]^+$ = 745.14), providing direct evidence that the Cu(III)-5,15-(*m*-nitrophenyl)-10-(*p*-trifluoromethylphenyl)corrole was successfully prepared. Similar parent peaks were also observed for **3b–d**.

The proton signals for the *meso*-substituents and pyrrole rings in the ^{1}H NMR spectra of **3a–d** lie beyond 7.40 ppm, and ^{19}F NMR spectra contain a singlet peak at δ = −62.57 ppm for **3a** and at δ = −62.63 ppm for **3b**, which is consistent with the presence of trifluoromethylphenyl rings at the *meso*-positions. The structure of the Cu(III)corrole was unambiguously elucidated through an X-ray structural analysis on single crystals of **3d** obtained through the slow diffusion of hexane into a toluene solution (Fig. 1 and Table S1, see the ESI†). The crystal adopts the $Pca2_1$ space group. The structure of **3d** is similar to that of other metallotriarylcorroles, which have a four-coordinate Cu(III) ion. The crystal structures (Fig. 1) exhibit Cu–N distances averaging around 1.9 Å, and the novel feature of the crystal structures is that the corrole macrocycle is significantly saddled (*i.e.*, the pyrrole rings are alternately tilted up and down from the mean plane). Although saddling is not unprecedented for copper corroles, the previous examples have involved sterically hindered derivatives such as the Cu(III) complexes of *meso*-triarylcorrole.[12]

Optical spectra and TD-DFT calculations

The electronic structures and optical spectra of porphyrinoids can be readily rationalized by using Gouterman's 4-orbital model[13] and Michl's perimeter model.[14] The π-MOs associated with the 15 atom 18 π-electron inner ligand perimeter are arranged in an M_L = 0, ±1, ±2, ±3, ±4, ±5, ±6, ±7 sequence in ascending energy terms that is determined by the angular nodal properties. Since the HOMO and LUMO have M_L values of ±4 and ±5, respectively, Gouterman's 4-orbital model predicts the presence of an allowed B transition (ΔM_L = ±1) at high energy and a forbidden Q transition (ΔM_L = ±9) at low energy. The B bands of **3a–d** can be readily assigned to the intense band in the 400–410 nm region and the shoulder of absorbance to high energy, since there is an intense pair of oppositely-signed Faraday $\mathbf{B_0}$ terms in the MCD spectra (Fig. 2).[8,15] A comparison with TD-DFT calculations provides further evidence for this (Fig. 3 and Table S2, see the ESI†). The analysis of the weaker bands in the Q band region (500–700 nm) is complicated by the presence of ligand-to-metal charge transfer (LMCT) bands, since the LUMO is predicted to be associated primarily with the $3d_{x^2-y^2}$ orbital of the central metal ion (Fig. 4).

In order to facilitate a comparison of complexes with differing symmetries without consulting correlation tables, Michl[14] referred to π-MOs derived from the HOMO and LUMO of the parent perimeter with angular nodal planes that lie on the *y*-axis as the **a** and **-a** MOs, respectively, while the corresponding MOs that have significant MO coefficients on the *y*-axis are referred to as the **s** and **-s** MOs (Fig. 4). The **-a** and **-s** MOs are predicted to be the LUMO+1 and LUMO+4, respectively, because there are two low-lying MOs localized on the A_2-position *meso*-substituents, while the **s** and **a** MOs are the HOMO and HOMO−1, respectively. The introduction of different B-position *meso*-aryl groups results in a destabilization or stabilization of the MO stack based on whether they have electron-donating or withdrawing inductive properties.

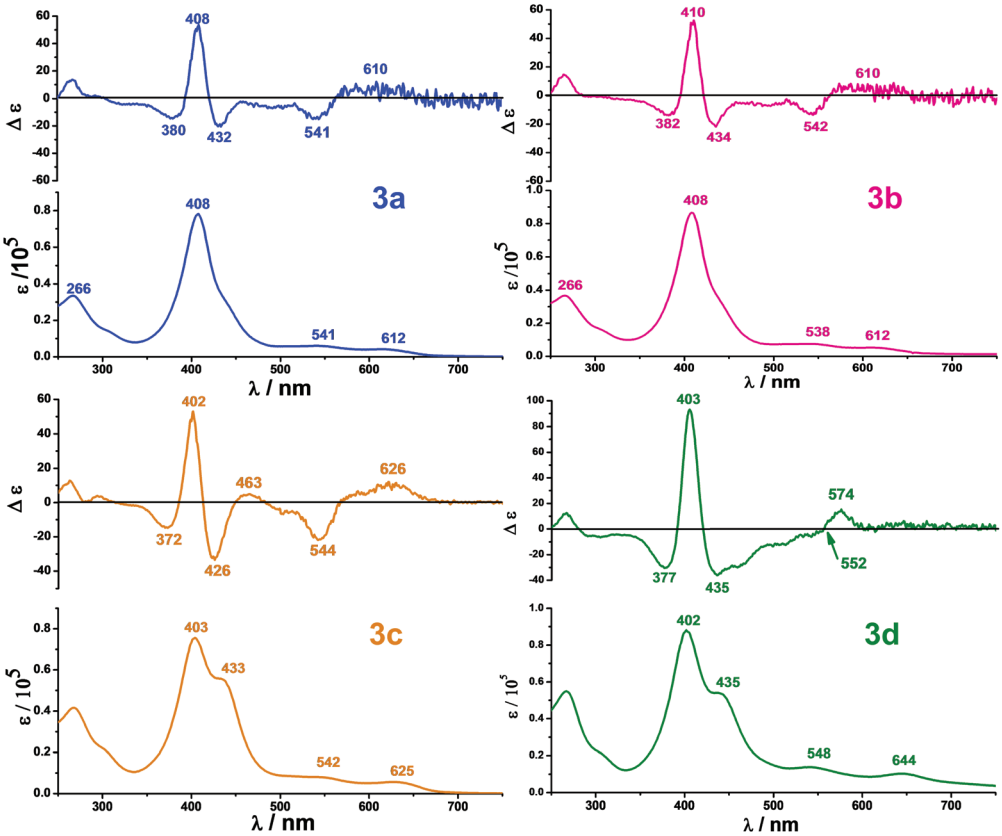

Fig. 2 UV-visible absorption (bottom) and magnetic circular dichroism (MCD, top) spectra of Cu(III)corroles **3a–d** at room temperature in CH_2Cl_2.

When electron donating substituents are added there is a relative destabilization of the HOMO, and this results in a slight narrowing of the HOMO–LUMO gaps of **3c** and **3d**. Since the effect of the *meso*-aryl rings is anticipated to primarily be an inductive rather than mesomeric one if the aryl ring does not lie coplanar with the porphyrin ligand and the HOMO and LUMO both significant MO coefficients at the three *meso*-carbons, there is no scope for the large changes in the HOMO–LUMO gap that have been reported for porphyrazines with other types of push–pull substitution patterns that result in a strong destabilization of the HOMO and a stabilization of the LUMO due to strong mesomeric interactions.[3] The trends observed in the predicted MO energies are therefore consistent with the relatively minor changes that are observed in the experimental and calculated optical spectra of **2a–d** (Fig. 2 and 3).

When compared to the Q band absorption of regular Cu(III)-*meso*-triphenyl-corroles with *meso*-nitrophenyl rings at the A_2-positions,[16] there is a sizeable red-shift of the lower energy band in the Q band region, at **3a**: 612 nm, **3b**: 612 nm, **3c**: 625 nm, and **3d**: 644 nm in CH_2Cl_2, and of the B band, at **3a**: 408 nm, **3b**: 410 nm, **3c**: 402 nm, and **3d**: 403 nm in CH_2Cl_2. Average HOMO–LUMO gap values were calculated by taking into account the energies of the **a**, **s**, **-a** and **-s** MOs that arise from the HOMO and LUMO of the $C_{15}H_{15}^{3-}$ parent perimeter, since all four of these MOs are involved with the Q and B bands (Table S1, see the ESI†). The HOMO–LUMO gap values for **3a–d** are very similar, so the significant wavelength shifts that are observed in the Q band region are probably due to configurational interactions with close-lying ligand-to-metal charge transfer (LMCT) states. In the B band region, there is a greater resolution of the *x*- and *y*-polarized components of the B transition in the case of **3c** and **3d**, with clear shoulders of intensity observed at 433 and 435 nm, respectively. The more complex −/+/− sign sequence that is observed in ascending energy terms in the B band region (432, 408 and 380 nm in the MCD spectrum of **3a**) is probably due to configurational interaction with a close-lying excited state with LMCT character. The absorption bands with lower intensity correspond to the blue of the nitrophenyl groups;[16] there is a facile one-electron reduction to generate a $[Cu(II)corrole]^-$ species during the 1st reduction and the main B band at *ca.* 409 nm can also be assigned in part as being LMCT in origin. Transitions to $\pi\pi^*$ states associated with the low-lying MOs that are associated with the A_2 *meso*-aryl rings are also predicted to lie in this region (Fig. 4). When the electron-donating ability of the B-position *meso*-substituent is increased in the context of **3c** and **3d**, there is a significant increase in the intensity of a broad absorption band at around 800–1200 nm (Fig. S1, see the ESI†) that can be assigned as the forbidden LMCT bands that are predicted to lie beyond 900 nm in the calculated TD-DFT spectra (Fig. 3).

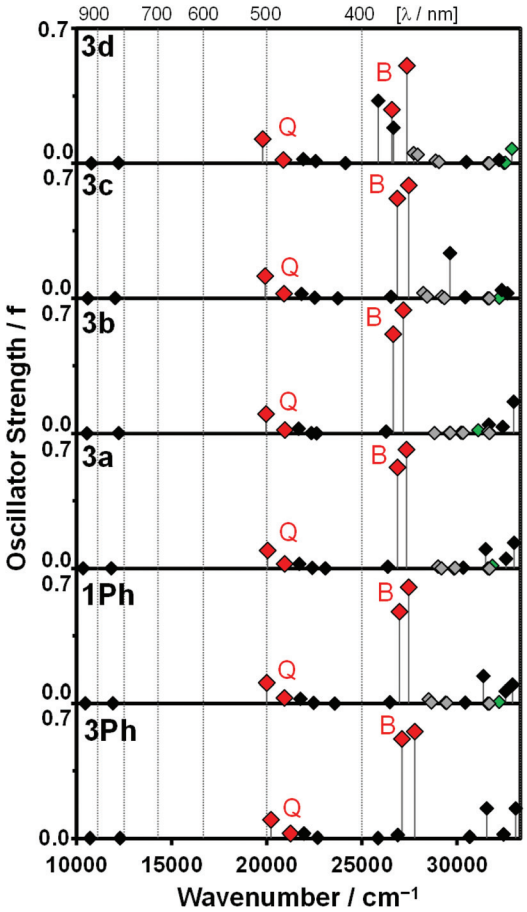

Fig. 3 The calculated TDDFT spectra for the **3Ph** and **1Ph** model compounds and **3a–d** calculated by using the CAM-B3LYP functional and 6-31G(d) basis sets for a series of B3LYP optimized geometries. Red and green diamonds are used to highlight the Q and B bands of Gouterman's 4-orbital model and bands associated with other low lying ππ* states, while black and gray diamonds are used for ligand-to-metal charge transfer (LMCT) bands associated with the LUMO and charge transfer bands associated with the LUMO+2 and LUMO+3 that are localized on the A_2-position *meso*-substituents, respectively.

Electrochemistry

In order to gain further insight into the electronic structures of **3a–d**, cyclic and differential pulse voltammetry (CV and DPV) measurements were carried out in *o*-dichlorobenzene (*o*-DCB) and PhCN containing 0.1 M tetra-*n*-butylammonium perchlorate ([NBu]ClO_4; TBAP) as a supporting electrolyte, so that redox potential ($E_{1/2}$) values could be derived in solvents of both low and high polarities (Fig. 5 and S2, see the ESI†). The electrochemical properties of **3a–d** in these solvents are similar to those reported for other Cu(III)corroles.[17] As has been reported previously for other metallo-corroles with two *meso*-steps, followed by a one-electron reduction on the *meso*-nitrophenyl rings for the 2nd step and a two-electron reduction on the *meso*-nitrophenyl rings and the oxidation of Cu(III)corrole to [Cu(III)corrole]$^+$ π cations are observed during the first oxidation. When both electron-donating and withdrawing substituents are introduced at the *meso*-positions, there is a decrease in the electron density on the π-conjugation system of the corrole ligand and an increase in the dipole moment of the complex.

The redox potentials (Table 1) are shifted considerably relative to those that have been reported previously for Cu(III)-*meso*-triarylcorroles with two nitrophenyl rings at the A_2-positions,[16] due to the push–pull substitution patterns at the *meso*-carbon positions. The cyclic voltammogram for **3b** with strongest electron-withdrawing substituents in this study has a first reversible [Cu(III)corrole]/[Cu(II)corrole]$^-$ reduction step at $E_{1/2}$ = 0.06 V (in *o*-DCB). There is a negative shift of the $E_{1/2}$ values for other complexes, which follows the trend in the electron-donating ability of the *meso*-aryl rings at the B-position on moving from **3a** to **3d** from **3a** (0.02 V) to **3c** (−0.05 V) and **3d** (−0.10 V), respectively. The trend observed in the gaps between the first reduction and oxidation steps is consistent with the slight blue-shift of the main Q and B bands that is observed spectroscopically for compounds with push–pull type *meso*-aryl substituents (Fig. 2) and predicted in theoretical calculations (Fig. 3), since the inductive effect of the *meso*-aryl rings on the energies of the frontier MOs is similar in each case. On the other hand, when the more polar PhCN was used as the solvent for the electrochemical measurements, the positive shift of the $E_{1/2}$ values is observed for all of the electrochemical processes, which shows that solvent polarity has a significant influence. Tafel plots can also be used to demonstrate that the efficiency of the electrocatalyzed HERs can be modulated in a rational manner. When Tafel plots are prepared for **3a–d** (Fig. S3, see the ESI†) the trends are similar to those observed for the other aspects of the electrochemical properties.

Spectroelectrochemistry

Spectroelectrochemical studies were carried out *in situ* in a thin layer cell in both *o*-dichlorobenzene (*o*-DCB) and PhCN containing 0.1 M TBAP to assist the further characterization of the oxidation and reduction products. In *o*-DCB, there is a decrease in intensity at 410 nm in the B band region as the singly reduced species of **3a** and **3b** is formed, while a new band at 440 nm gains intensity, along with a visible region band at *ca.* 620 nm (Fig. S4, see the ESI†). When the electron donating properties of the B-position *meso*-substituent are increased, the visible region absorption band shifts to *ca.* 645 nm for **3c**, while bands are observed at 613 and *ca.* 750 nm for **3d**. This process can be assigned to a reduction at the metal-center to form a [Cu(II)corrole]$^-$ species, and the different morphologies of the absorption bands can be attributed to the push–pull effects that are introduced by the *meso*-aryl substituents.

Oxidation of the metal ion is not anticipated based on the predicted MO energies, so the first oxidation steps of **3a–c** in *o*-DCB are expected to result in the formation of a ring-oxidized [Cu(III)corrole]$^+$ π-cation species, since the HOMO is a π-MO (Fig. 4).[12b,18] A similar set of spectral changes is observed in each case. There is a decrease in intensity in the Q and B band regions, while there is an increased intensity beyond 680 nm and in the NIR region, as would normally be expected after the formation of a π-cation.[12b,18] It should be noted that

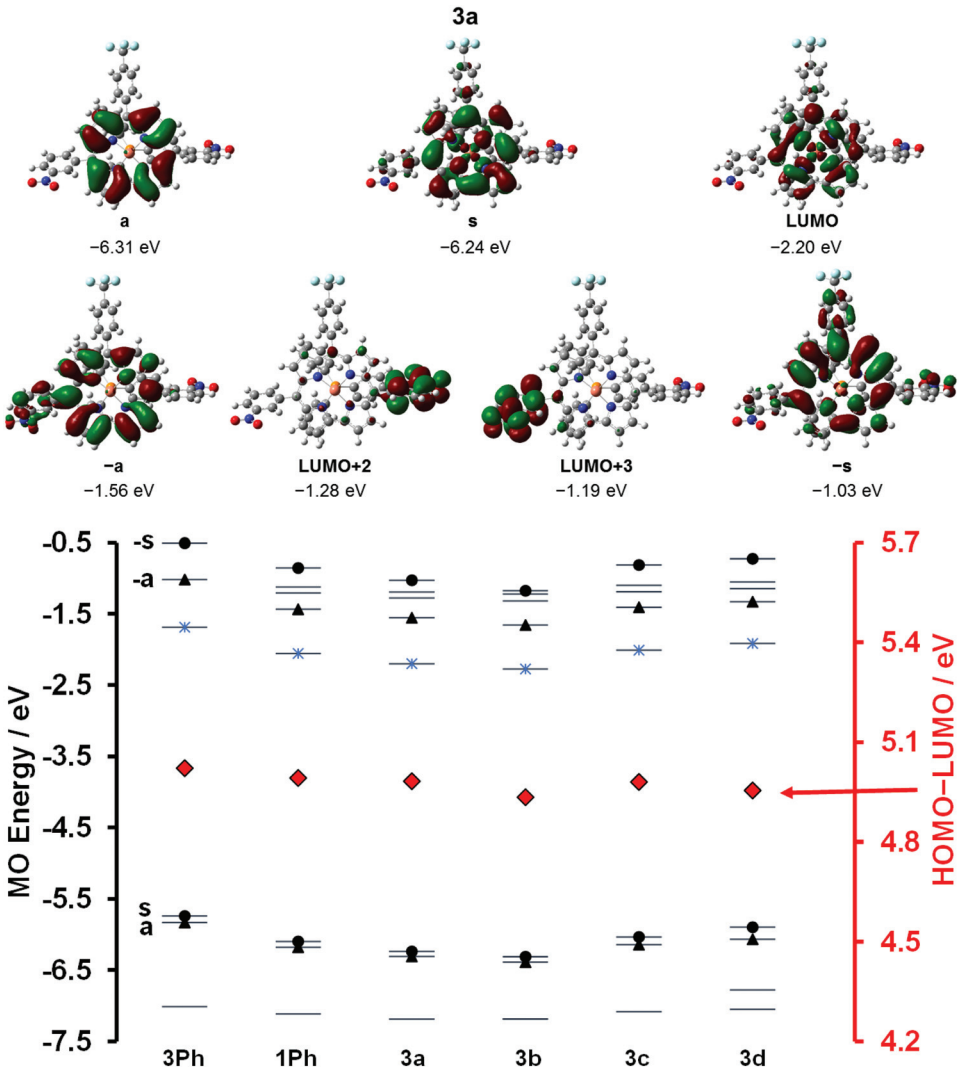

Fig. 4 The angular nodal patterns of the LUMO, LUMO+2, and LUMO+3 of **3a** and the **a**, **s**, **-a** and **-s** MOs of Michl's perimeter model that are associated with the 15 atom 18 π-electron inner ligand perimeter (top). MO energies predicted for the **3Ph** and **1Ph** model compounds and **3a–d** calculated by using the CAM-B3LYP functional and 6-31G(d) basis sets for a series of B3LYP optimized geometries (bottom). Black triangles and circles are used to highlight the **a**/**-a** and **s**/**-s** MOs, respectively, while a blue star is used to highlight the LUMO, which has significant $3d_{x^2-y^2}$ orbital character. Red diamonds are used to highlight the HOMO–LUMO gap values, which are plotted on a secondary axis.

in the case of **3d**, the neutral complex absorbs relatively strongly in the NIR region (Fig. S1, see the ESI†) due to the presence of the LMCT bands that are predicted in the calculated TD-DFT spectra (Fig. 3). This is probably related to the strong dipole moment in the ground state that is associated with the push–pull *meso*-substitution pattern. When the solvent polarity was increased by using PhCN rather than *o*-DCB, a shift of the B-band absorption is observed along with an increase in the Q-band intensity (Fig. S4, see the ESI†). No significant differences were observed during the first oxidation step, however.

HER catalysis

Stability in acidic environments is an important consideration during the design of new HER catalysts. The stability of **3a–d** was evaluated at high trifluoroacetic acid (TFA) concentrations (Fig. S5, see the ESI†). The Cu(III)corroles and TFA (1 : 4 molar ratio) were mixed in PhCN and were kept in the dark. Electronic absorption spectra were recorded at regular intervals for 4 h. Since negligible spectral changes are observed, it is safe to assume that **3a–d** are suitable for use as HER catalysts. Upon addition of 1.0 eq. of TFA to solutions of **3a–d**, there is a significant increase in the peak current (i_{cat}) at *ca.* $E = -1.0$ V (Fig. 6). The intensities of these peaks at around $E = -0.9$ V are much stronger than those observed when only the Cu(III)triarylcorroles and TFA are present in solution. It should be noted that a slight change in the potential values of **3d** was observed due to the protonation of the dimethylaminophenyl-unit at the B-position. An analysis of the i_{cat} values derived from CV measurements for **3a–d** in the presence of 1.0 eq. of

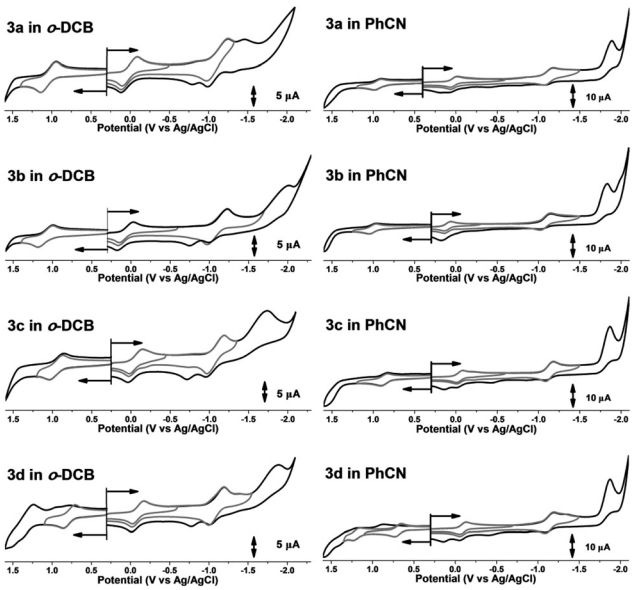

Fig. 5 CV measurements for **3a–d** in *o*-DCB (left) and PhCN (right) containing 0.1 M $[NBu_4]^+[ClO_4]^-$ (TBAP) as a supporting electrolyte.

Table 1 Potential values of **3a–d** in *o*-DCB and PhCN

	Solvent	$1^{st}\ E_{1/2}^{Ox2}$	$1^{st}\ E_{1/2}^{Red}$	$2^{nd}\ E_{1/2}^{Red2}$
3a	*o*-DCB	1.04	0.02	−1.08
	PhCN	0.97	0.06	−1.10
3b	*o*-DCB	1.08	0.06	−1.08
	PhCN	1.01	0.10	−1.09
3c	*o*-DCB	0.95	−0.05	−1.06
	PhCN	0.95	0.04	−1.13
3d	*o*-DCB	0.78	−0.10	−1.10
	PhCN	0.70	−0.09	−1.15

TFA when the scan-rates were varied from 20–500 mV s^{-1} (Fig. S6, see the ESI†) provides an insight into the reversibility of the system on the experimental time-scale. The observed strong linear correlations confirm that the electrochemically catalyzed hydrogen evolution processes are diffusion controlled.

The kinetic reactivity (i_{cat}/i_p) and onset potentials can be used to evaluate the efficiency of the HERs (Fig. 7). The addition of TFA to homogeneous solutions of **3a–d** in PhCN induces catalytic waves beyond the Cu^{III}/Cu^{II} and Cu^{II}/Cu^{I} reduction couples. When the concentration of TFA is increased from 1.0–8.0 eq., there is a clear increase in the i_{cat} values that is related to the electron-withdrawing ability of the B-position *meso*-substituent, which demonstrates that the push–pull properties of A_2B type corroles have a significant influence on HER catalysis. The catalytic wave increases in amplitude when the acid concentration is increased and progressively shifts to more negative potentials. In the case of **3b**, the complex with the most strongly electron-withdrawing B-position *meso*-substitution was found to be the most efficient catalyst (with a maximum i_{cat} value of 3.5×10^{-5} A), followed in order of efficiency by **3a**, **3c** and **3d** since there is an increase in the electron donating ability of the B-position *meso*-substituent in this order.

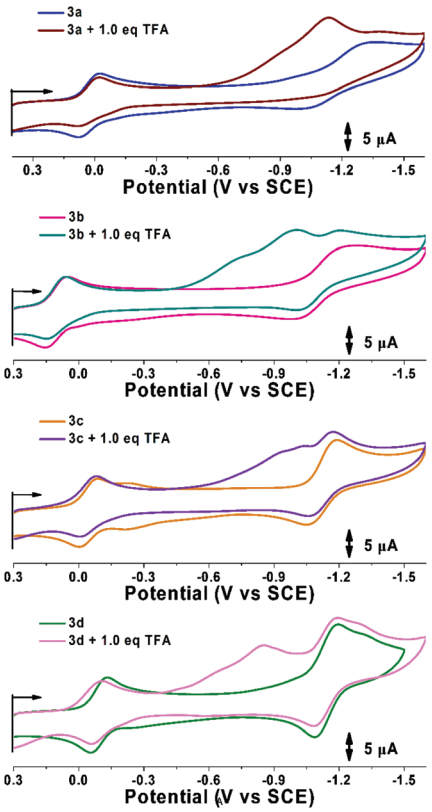

Fig. 6 Reductive electrochemical measurements of Cu(III)corroles **3a–d** in the absence and presence of 1.0 eq. of TFA in PhCN containing 0.1 M $[NBu_4]^+[ClO_4]^-$ (TBAP) as a supporting electrolyte.

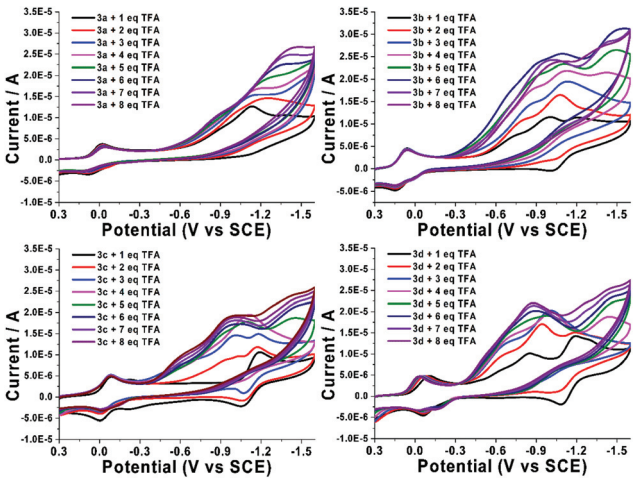

Fig. 7 Reductive electrochemical measurements of Cu(III)corroles **3a–d** in the presence of 1.0–8.0 eq. of TFA in PhCN containing 0.1 M $[NBu_4]^+[ClO_4]^-$ (TBAP) as a supporting electrolyte.

Conclusions

A series of Cu(III)triarylcorroles containing asymmetric push–pull *meso*-substitutions have been synthesized and characterized. A detailed analysis of the UV-visible absorption and MCD spectra, cyclic and differential pulse voltammetry measurements, *in situ* thin-layer electrochemical characterization, and the results of DFT and TD-DFT calculations has been carried out to identify the key trends in the redox and optical properties. Evidence for normally forbidden LMCT bands associated with the Cu(III) ion was observed in the NIR region of the optical spectra of **3d**, which has the strongest push–pull properties. This study demonstrates that A_2B type Cu(III)triarylcorroles are highly efficient catalysts for HER applications and that the catalytic properties can be readily modified by adjusting the push–pull properties of the *meso*-aryl rings, but the best results are obtained by having strongly electron-withdrawing aryl groups at all three *meso*-positions rather than having an electron-donating group at the B-position.

Acknowledgements

Financial support was provided by the NSFC of China (no. 21171076) and NSFC of Jiangsu province (no. BK20160449) to XL and WZ, and an NRF of South Africa CSUR grant (93627) to JM. The theoretical calculations were carried out at the Centre for High Performance Computing in Cape Town.

References

1 H. B. Gray, *Nat. Chem.*, 2009, **1**, 7.
2 D. Wöhrle and D. Meissner, *Adv. Mater.*, 1991, **3**, 129.
3 (*a*) X. Liang, S. Shimizu and N. Kobayashi, *Chem. Commun.*, 2014, **50**, 13781; (*b*) V. N. Kopranenkov, L. S. Goncharova and E. A. Luk'yanets, *Zh. Obshch. Khim.*, 1979, **49**, 1408; (*c*) A. R. Morgan, N. H. Petousis and J. E. van Lier, *Eur. J. Med. Chem.*, 1997, **32**, 21; (*d*) S. Shimizu, Y. Haseba, M. Yamazaki, G. Kumazawa and N. Kobayashi, *Chem. – Eur. J.*, 2014, **20**, 4822; (*e*) J. Mack and N. Kobayashi, *Chem. Rev.*, 2011, **111**, 281.
4 (*a*) T. R. Cook, D. K. Dogutan, S. Y. Reece, Y. Surendranath, Y. T. S. Teets and D. G. Nocera, *Chem. Rev.*, 2010, **110**, 6474; (*b*) J. L. Dempsey, B. S. Brunschwig, J. R. Winkler and H. B. Gray, *Acc. Chem. Res.*, 2009, **42**, 1995; (*c*) A. LeGoff, V. Artero, B. Jousselme, P. D. Tran, N. Guillet and R. Mataye, *Science*, 2009, **326**, 1384; (*d*) F. Wang, W. G. Wang, H. W. Wang, G. Si, C. H. Tung and L. Z. Wu, *ACS Catal.*, 2012, **2**, 407; (*e*) Z. J. Han, F. Qiu, R. Eisenberg, P. L. Holland and T. D. Krauss, *Science*, 2012, **338**, 1321; (*f*) E. S. Andreiadis, P. A. Jacques, P. D. Tran, A. Leyris, M. Chavarot-Kerlidou and B. Jousselme, *Nat. Chem.*, 2013, **5**, 48.
5 (*a*) S. Dey, A. Rana, S. G. Dey and A. Dey, *ACS Catal.*, 2013, **3**, 429; (*b*) B. H. Solis, A. G. Maher, T. Honda, D. C. Powers, D. G. Nocera and S. Hammes-Schiffer, *ACS Catal.*, 2014, **4**, 4516; (*c*) L. J. Chen, G. Chen, C. F. Leung, S. M. Yiu, C. C. Ko and E. Anxolabehere-Mallart, *ACS Catal.*, 2015, **5**, 356.
6 (*a*) M. L. Helm, M. P. Stewart, R. M. Bullock, M. R. DuBois and D. L. DuBois, *Science*, 2011, **333**, 863; (*b*) W. H. Zhu, T. T. Huang, M. F. Qin, M. Z. Li, J. Mack and X. Liang, *J. Electroanal. Chem.*, 2016, **774**, 58; (*c*) M. Z. Li, L. L. Liang, C. Ni, X. Liang and W. H. Zhu, *J. Electroanal. Chem.*, 2016, **766**, 135; (*d*) Y. Jiang, M. Z. Li, X. Liang, J. Mack, M. Wildervanck, T. Nyokong, M. F. Qin and W. H. Zhu, *Dalton Trans.*, 2015, **44**, 18237; (*e*) M. J. Rose, H. B. Gray and J. R. Winkler, *J. Am. Chem. Soc.*, 2012, **134**, 8310; (*f*) C. L. Pitman and A. J. M. Miller, *ACS Catal.*, 2014, **4**, 2727.
7 (*a*) J. G. Kleingardner, B. Kandemir and K. L. Bren, *J. Am. Chem. Soc.*, 2014, **136**, 4; (*b*) I. Bhugun, D. Lexa and J. Saveant, *J. Am. Chem. Soc.*, 1996, **118**, 3982; (*c*) V. Grass, D. Lexa and J. Saveant, *J. Am. Chem. Soc.*, 1997, **119**, 7526; (*d*) A. Rana, B. Mondal, P. Sen, S. Dey and A. Dey, *Inorg. Chem.*, 2017, **56**, 1783–1793; (*e*) H. T. Lei, H. Y. Fang, Y. Z. Han, W. Z. Lai, X. F. Fu and R. Cao, *ACS Catal.*, 2015, **5**, 5145; (*f*) M. Z. Li, Y. J. Niu, W. H. Zhu, J. Mack, T. Nyokong and X. Liang, *Dyes Pigm.*, 2017, **137**, 523; (*g*) B. Mondal, K. Sengupta, A. Rana, A. Mahammed, M. Botoshansky, S. G. Dey, Z. Gross and A. Dey, *Inorg. Chem.*, 2013, **52**, 3381; (*h*) A. Mahammed, B. Mondal, A. Rana, A. Dey and Z. Gross, *Chem. Commun.*, 2014, **50**, 2725.
8 (*a*) S. B. Piepho and P. N. Schatz, in *Group Theory in Spectroscopy with Applications to Magnetic Circular Dichroism*, Wiley, New York, 1983; (*b*) J. Mack, M. J. Stillman and N. Kobayashi, *Coord. Chem. Rev.*, 2007, **251**, 429.
9 G. M. Sheldrick, *SHELXS-97, Program for X-ray Crystal Structure Determination*, University of Göttingen, Germany, 1997.
10 M. J. Frisch, G. W. Trucks, H. B. Schlegel, G. E. Scuseria, M. A. Robb, J. R. Cheeseman, G. Scalmani, V. Barone, B. Mennucci, G. A. Petersson, H. Nakatsuji, M. Caricato, X. Li, H. P. Hratchian, A. F. Izmaylov, J. Bloino, G. Zheng, J. L. Sonnenberg, M. Hada, M. Ehara, K. Toyota, R. Fukuda, J. Hasegawa, M. Ishida, T. Nakajima, Y. Honda, O. Kitao, H. Nakai, T. Vreven, J. A. Montgomery Jr., J. E. Peralta, F. Ogliaro, M. Bearpark, J. J. Heyd, E. Brothers, K. N. Kudin, V. N. Staroverov, R. Kobayashi, J. Normand, K. Raghavachari, A. Rendell, J. C. Burant, S. S. Iyengar, J. Tomasi, M. Cossi, N. Rega, M. J. Millam, M. Klene, J. E. Knox, J. B. Cross, V. Bakken, C. Adamo, J. Jaramillo, R. Gomperts, R. E. Stratmann, O. Yazyev, A. J. Austin, R. Cammi, C. Pomelli, J. W. Ochterski, R. L. Martin, K. Morokuma, V. G. Zakrzewski, G. A. Voth, P. Salvador, J. J. Dannenberg, S. Dapprich, A. D. Daniels, Ö. Farkas, J. B. Foresman, J. V. Ortiz, J. Cioslowski and D. J. Fox, *Gaussian 09, Revision D.01*, Gaussian, Inc., Wallingford, CT, 2009.
11 M. Z. Li, W. H. Zhu, J. Mack, S. Mkhize, T. Nyokong and X. Liang, *Chin. J. Struct. Chem.*, 2017, **36**, 367–380.

12 (*a*) A. B. Alemayehu, E. Gonzalez, L. K. Hansen and A. Ghosh, *Inorg. Chem.*, 2009, **48**, 7794; (*b*) G. Pomarico, X. Xiao, S. Nardis, R. Paolesse, F. R. Fronczek, K. M. Smith, Y. Y. Fang, Z. P. Ou and K. M. Kadish, *Inorg. Chem.*, 2010, **49**, 5766; (*c*) M. Stefanelli, F. Mandoj, M. Mastroianni, S. Nardis, P. Mohite, F. R. Fronczek, K. M. Smith, K. M. Kadish, X. Xiao, Z. P. Ou, P. Chen and R. Paolesse, *Inorg. Chem.*, 2011, **50**, 8281; (*d*) M. Stefanelli, M. Mastroianni, S. Nardis, S. Licoccia, F. R. Fronczek, K. M. Smith, W. H. Zhu, Z. P. Ou, K. M. Kadish and R. Paolesse, *Inorg. Chem.*, 2007, **46**, 10791.

13 M. Gouterman, in *The Porphyrins*, ed. D. Dolphin, Academic Press, New York, 1978; vol. III, Part A, pp. 1–165.

14 (*a*) J. Michl, *J. Am. Chem. Soc.*, 1978, **100**, 6801; (*b*) J. Michl, *Pure Appl. Chem.*, 1980, **52**, 1549; (*c*) J. Michl, *Tetrahedron*, 1984, **40**, 3845.

15 (*a*) N. Kobayashi, A. Muranaka and J. Mack, *Circular Dichroism and Magnetic Circular Dichroism Spectroscopy for Organic Chemists*, Royal Society of Chemistry, Cambridge, 2011; (*b*) P. J. Stephens, *Adv. Chem. Phys.*, 1976, **35**, 197.

16 B. H. Li, Z. P. Ou, D. Y. Meng, J. J. Tang, Y. Y. Fang, R. Liu and K. M. Kadish, *J. Inorg. Biochem.*, 2014, **136**, 130.

17 (*a*) K. M. Kadish, V. A. Adamian, E. Van-Caemelbecke, E. Gueletii, S. Will, C. Erben and E. Vogel, *J. Am. Chem. Soc.*, 1998, **120**, 11986; (*b*) B. Sridevi, S. J. Narayanan, T. K. Chandrashekar, U. Englich and K. Ruhlandt-Senge, *Chem. – Eur. J.*, 2000, **6**, 2554; (*c*) I. H. Wasbotten, T. Wondimagegn and A. Ghosh, *J. Am. Chem. Soc.*, 2002, **124**, 8104; (*d*) R. Guilard, C. P. Gros, J. M. Barbe, E. Espinosa, F. Jerome, A. Tabard, J. M. Latour, J. Shao, Z. Ou and K. M. Kadish, *Inorg. Chem.*, 2004, **43**, 7441; (*e*) S. Will, J. Lex, E. Vogel, H. Schmickler, J. P. Gisselbrecht, C. Haubtmann, M. Bernard and M. Gross, *Angew. Chem., Int. Ed. Engl.*, 1997, **36**, 357; (*f*) A. Ghosh, T. Wondimagegn and A. B. Parusel, *J. Am. Chem. Soc.*, 2000, **122**, 5100; (*g*) E. Steene, A. Dey and A. Ghosh, *J. Am. Chem. Soc.*, 2003, **125**, 16300.

18 (*a*) Z. P. Ou, J. G. Shao, H. Zhao, K. Ohkubo, I. H. Wasbotten and S. Fukuzumi, *J. Porphyrins Phthalocyanines*, 2004, **8**, 1236; (*b*) G. F. Lu, W. S. Lin, Y. Y. Fang, W. H. Zhu, X. L. Ji and Z. P. Ou, *J. Porphyrins Phthalocyanines*, 2011, **15**, 1265.